Cavitation Mode Analysis of Pump Inducer

Seungbae Lee*, Keun-Hwa Jung
School of Mechanical Engineering, Inha University,
253 Yonghyun-dong, Nam-gu, Incheon 402-751, Korea
Jin-Hwa Kim, Shin-Hyoung Kang
School of Mechanical and Aerospace Engineering, Seoul National University,
San 56-1, Sillim-dong, Kwanak-gu, Seoul 151-742, Korea

The onset of cavitation causes head and efficiency of a main pump to be reduced significantly and generates vibration and noise. In order to avoid these phenomena, the inlet of the pump is fitted with a special rotor called an inducer, which can operate satisfactorily with extensive cavitation. The motivation of this study is to find out cavitation modes from the inducer inlet pressure signals and event characteristics from outlet ones at various operating conditions. The cavitation modes are analyzed by using a cross-spectral density of fluctuating pressures at the inducer inlet. The time-frequency characteristics of wall pressures downstream of the inducer are presented in terms of event frequency, its duration time, and number of events by using the Choi-Williams distribution.

Key Words : Cavitation, Pump Inducer, Event Detection Technique, Modified Cavitation Number

Nomenclature

BPF : Blade passage frequency (Hz)
C : Absolute velocity (m/s)
D : Diameter of impeller (m)
f : Frequency (Hz)
f_n : Shaft rotational speed (rps)
g : Gravity constant (m/s^2)
H : Actual head (m)
N : Rotational speed (rpm)
NPSH : Net Positive Suction Head
P : Pressure (Pa)
Q : Flow rate (m^3/min)
S : Pitch length (m)
St : Strouhal number (f/BPF)
U : Peripheral velocity (m/s)
W : Relative velocity (m/s)

Greeks

α : Incidence angle (°)
δ : Phase angle
η : Efficiency
ρ : Density (kg/m^3)
σ : Inlet cavitation number ($=P_1-P_{vap}$)/ ($\rho W_1^2/2$)
σ_c : Cross flow cavitation number ($=P_1-P_{vap}$)/ ($\rho W_{ct}^2/2$)
Φ : Flow coefficient (Q/ND^3) or Kernel function
λ : Sweep angle at tip
Ψ : Pressure coefficient (gH/N^{2}D^2)

Subscripts

1 : Inducer inlet
2 : Inducer outlet
a : Available NPSH
c : Component normal to the meridional view of leading edge
ct : Component approaching the cascade in the cross flow plane
d : Design point
m : Number of cavity

* Corresponding Author,
E-mail : sbaelee@inha.ac.kr
TEL : +82-32-860-7325; **FAX** : +82-32-868-1716
School of Mechanical Engineering, Inha University, 253 Yonghyun-dong, Nam-gu, Incheon 402-751, Korea.
(Manuscript **Received** February 27, 2002; **Revised** July 30, 2002)

n   : Component normal to the cascade blade
p   : Component parallel to the meridional view
      of leading edge
r   : Required NPSH
t   : Tip or Tangential component to blade sur-
      face
vap : Vapor
σ : Cavity
∞ : Mean

1. Introduction

Pure cavitation occurs when the local absolute static pressure of a liquid is lower than the vapor pressure of working fluid and causes vapor pockets. This phenomenon is strongly influenced by air content, curvature and geometry of blades as well as vapor pressure. Thus, it is very difficult to predict the inception point of cavitation which deteriorates performance and efficiency, and causes vibration and noise. While the surface cavitation of vapor bubbles occurs near the blade surface, the vortex cavitations are found in the forms of tip vortex, trailing vortex and secondary vortex. Such vortex cavitation generates a large cavitation cloud with many small cavitation bubbles (Kubota et al., 1989).

There have been many attempts to reduce damage by incorporating an inducer, which had a high-solidity, a large-stagger-angle and fewer-blades. Multistage pumps have been also successfully built with inducers, which accepted low pressure from a tank and increased the head sufficiently to avoid cavitation.

It is well-known that the cavitation mode of inducer depends not only on the flow coefficient, but also on cavitation number. It has been shown by Acosta (1955) that the cavity development is a function of $\sigma/2\alpha$. The tip vortex cavitation is often observed at a higher inlet pressure than that of steady cavitation or unsteady rotating cavitation in a typical inducer.

The steady surface cavitation of the inducer may be divided into equal length and alternate blade cavitation. It was found that when the cavity length increased to approximately 65% of the blade spacing, the mode change from equal

length to alternate blade cavitation might occur by interaction of blade suction surface of cavity with the leading edge of the next blade (Horiguch, et al., 2000).

The leading edge sweep was shown to make the ranges of alternate blade cavitation and unsteady cavitation shift toward lower cavitation number by reducing cavity length. Yoshida et al. reported the effects of alternate leading-edge-cutback design on suppression of rotating cavitation. The previous observations have been based on the spectral analysis of inlet pressure fluctuations aided by high-speed video pictures.

In this study, the pressure fluctuations at each cavitating condition were measured at inducer inlet and outlet locations using pressure transducers, which were located 90 degrees apart from each other to identify the cavitation modes. The time-frequency characteristics were analyzed by a local time-frequency analysis with Choi-Williams distribution for a four-bladed inducer of the same design as LE-7 liquid oxygen turbopump inducer and an axial inducer of industrial application.

2. Experimental Setup

The present experiments are conducted by using two types of inducer. The inducer A is designed and fabricated as shown in Fig. 1(a). The inducer A has two helical blades of axial configuration with a flat part near the leading edge and a circular arc in the rest of the chord. The inducer B has four helical blades on the hub having gradually increasing radii downstream, which is the same basic model as the one used at
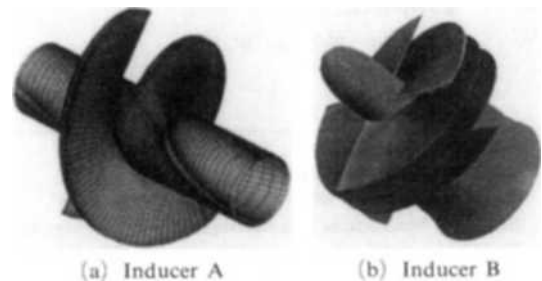

(a) Inducer A   (b) Inducer B

Fig. 1 Geometric view of inducers tested

Table 1 Geometric parameters of test inducer A

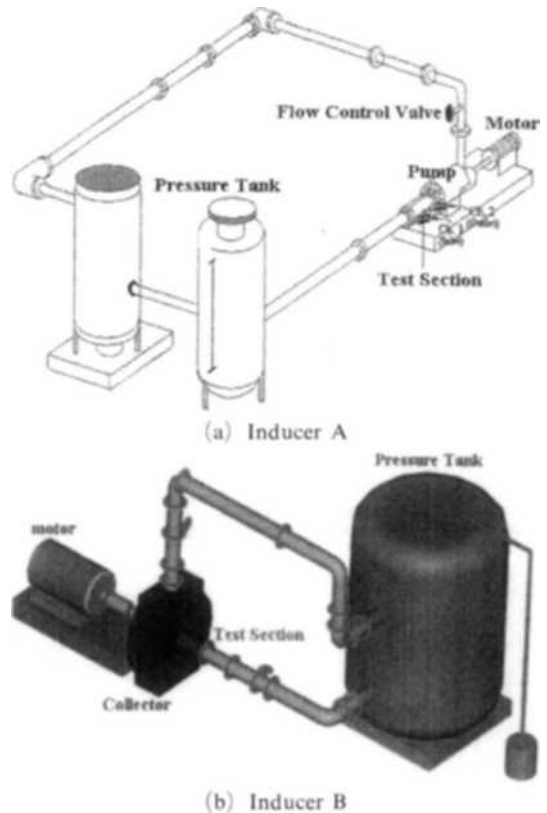|	Nomenclature	Size	Unit
1	Tip diameter	176.0	mm
2	Hub diameter	60.0	mm
3	Tip clearance	0.13	mm
4	Solidity at tip	2.06	
5	Inlet tip blade angle	13.5	deg.
6	Outlet tip blade angle	19.5	deg.
7	Blade number	2	
8	Blade thickness at tip	6	mm

Table 2 Geometric parameters of test inducer B

	Nomenclature	Size	Unit
1	Tip diameter	149.8	mm
2	Hub/tip ratio at inlet	0.25	
3	Hub/tip ratio at outlet	0.51	
4	Tip clearance	0.5	mm
5	Solidity at tip	2.97	
6	Inlet tip blade angle	7.5	deg.
7	Outlet tip blade angle	9.0	deg.
8	Blade number	4	
9	Blade thickness at tip	2	mm

(a) Inducer A

(b) Inducer B

Fig. 2 Schematic of experimental apparatus

LE-7 engine of H-2 rocket in Japan as shown in Fig. 1(b). While the inducer A has zero leading edge sweep, the leading edge of inducer B is 47.3° swept backward. The geometric details of each inducer are given in Table 1 and 2, respectively. These are installed ahead of centrifugal pumps.

Figure 2(a) shows the schematic of test facility for the inducer A. It consists of a test section, an inducer, a collector, gate valves, a pressure vessel, and flow-control valves in a closed loop. For NPSH measurement, the vacuum pressure of the pressure vessel is adjusted. The casing of test section is made of transparent acrylic resin.

The experimental apparatus of inducer B as shown in Fig. 2(b) supplies degassed water from the pressure vessel to the inducer. The cavitation modes are observed by controlling the inlet pressure of inducer through the vacuum pump installed at the top of pressure vessel.

In both test rigs, inlet pressure fluctuations are measured by using two 1/2″ pressure transducers

(Trans-Metrics Model P037D) at circumferential locations with 90° separation to identify types of cavitation modes. The outlet pressure fluctuations are measured by changing the flow-coefficient and cavitation number systematically. The power spectra of fluctuating wall pressures are obtained by using an FFT analyzer to determine the spectral features of ensemble-averaged data from more than 3,000 events. The random error, ε_d, computed from $1/\sqrt{n_d}$ is about $\pm 1.8\%$. The fluctuating pressures are also sampled with an A/D converter at a sampling rate of 30 kHz per channel and processed with Labview®.

3. Inducer Cavitation Performance

Figure 3(a) and (b) show non-cavitating performance of the inducer A combined with a centrifugal pump in terms of total head and efficiency. The design point of the inducer A is
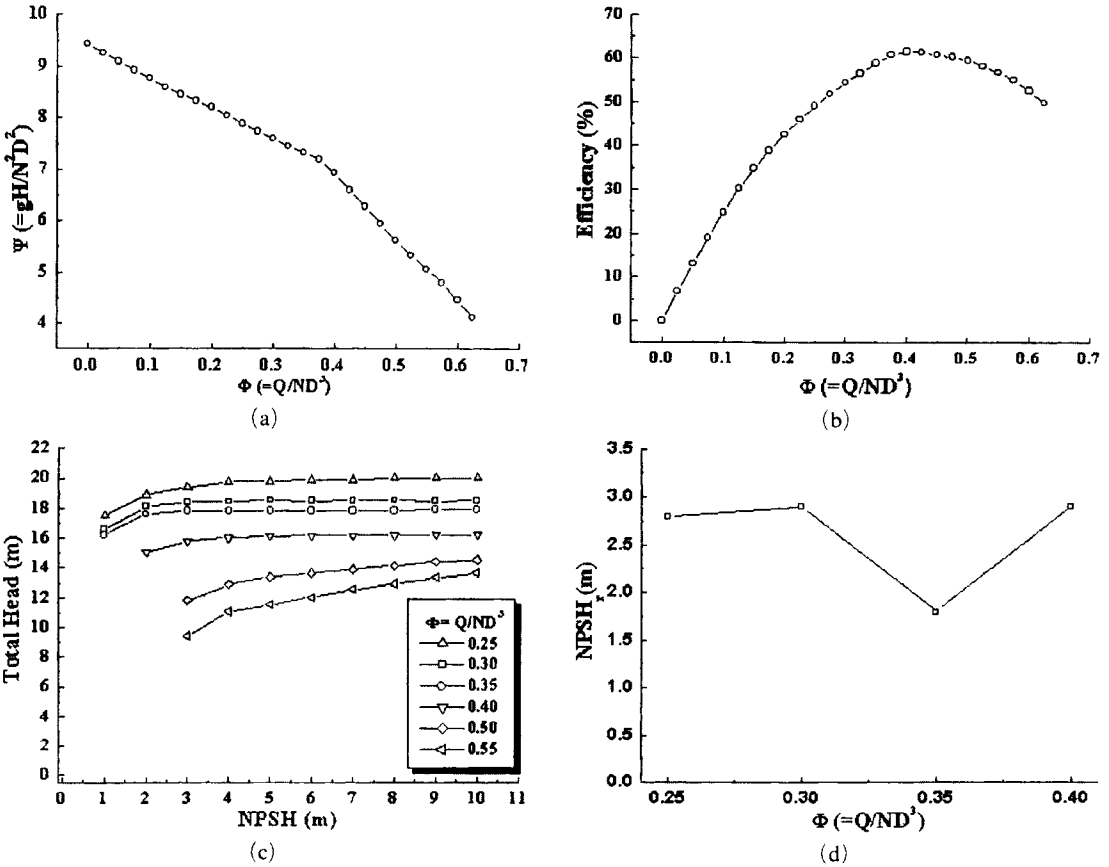
Fig. 3 Characteristic curves of inducer A and pump, (a) static pressure performance ; (b) efficiency ; (c) suction head performance (NPSH$_a$) at constant ; (d) cavitation inception by 3% head reduction

near Φ_d=0.4. Figure 4(a) and (b) show non-cavitating static pressure performance of the inducer B alone. The head coefficient of the inducer decreases linearly with an increasing flow coefficient. The design flow rate is found near Φ_d= 0.15.

The cavitation performance of a turbomachine can be represented by Net Positive Suction Head (NPSH) defined as Eq. (1) and cavitation number defined by Eq. (2).

$$NPSH = \frac{P_1}{\rho g} + \frac{C_1^2}{2g} - \frac{P_{vap}}{\rho g} \qquad (1)$$

$$\sigma = \frac{P_1 - P_{vap}}{1/2\rho W_1^2} \qquad (2)$$

The total head variations of inducers A and B are plotted in terms of NPSH at some fixed flow coefficients in Figs. 3(c) and 4(c), respectively.

Figures 3(d) and 4(d) show the inception points of cavitation based on 3% head reduction at each flow coefficient. As shown, the design points have the minimal values in NPSH$_r$. This suggests that the inducer at the design point is more resistable to cavitation than at off-design points.

Let the pressure in the cavity be P_{vap} and the velocity be W_c. By applying the Bernoulli equation to inlet and passage locations :

$$P_1/\rho + W_1^2/2 = P_{vap}/\rho + W_\sigma^2/2 \qquad (3)$$

Combining Eqs. (2) and (3), we have the cavity velocity as follows :

$$W_\sigma = W_1\sqrt{1+\sigma} \qquad (4)$$

If we consider the relative velocity in the cross plane approaching the cascade (Yoshida et al., 2001), we have the total velocity (W_{ct}) and cross-flow cavitation number (σ_c) as $\sqrt{(W_c^2 + W_n^2)}$ and
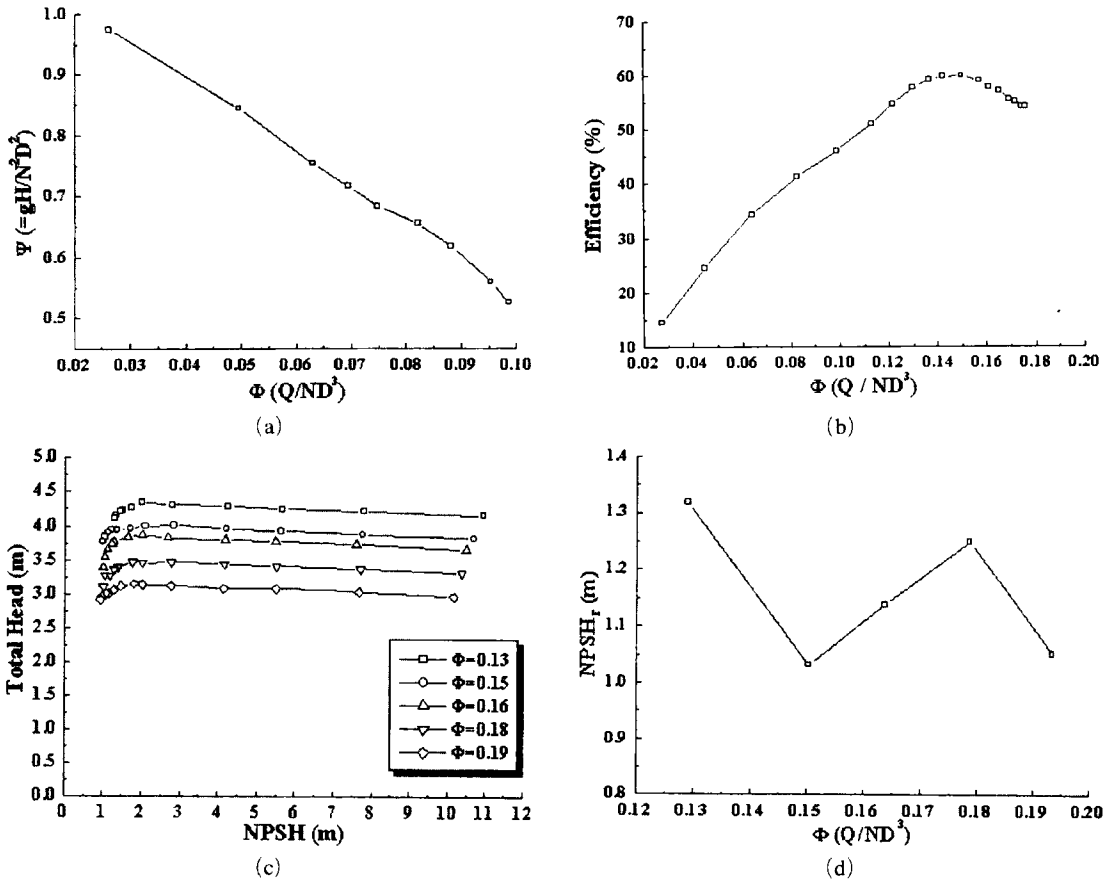
Fig. 4 Characteristic curves of inducer B. (a) static pressure performance; (b) efficiency; (c) suction head performance (NPSH$_a$) at constant Φ; (d) cavitation inception by 3% head reduction
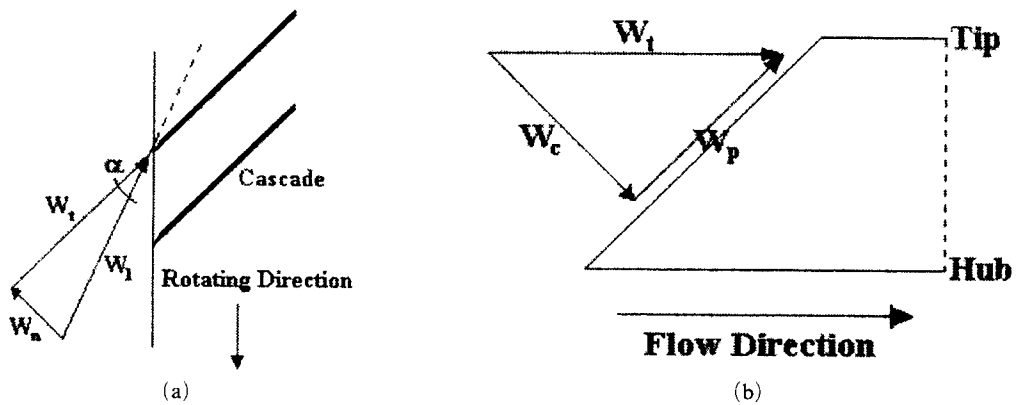

Fig. 5 Schematic view of velocity vectors in swept cascades, (a) Plan view; (b) Meridional view

$(P_1-P_{vap})/(\rho W_{ct}^2/2)$, respectively. For a typically small incidence angle of α less than 1.0, $\sigma_c \approx \sigma/\sin^2 \lambda$, where λ is the leading-edge sweep angle at tip. The velocity vectors in the swept cascade used in this study are schematically shown in Fig. 5. The cavitation parameters at

Table 3　Cavitation parameters at each tested case for tested impellers

Inducer A				Inducer B							
$\Phi=0.30$		$\Phi=0.35$		$\Phi=0.10$				$\Phi=0.13$			
σ	$\sigma/2\alpha$	σ	$\sigma/2\alpha$	σ	σ_c	$\sigma/2\alpha$	$\sigma_c/2\alpha_c$	σ	σ_c	$\sigma/2\alpha$	$\sigma_c/2\alpha_c$
0.3	1.26	0.3	1.56	0.32	0.93	1.79	3.05	0.32	0.93	2.13	3.64
0.17	0.73	0.17	0.9	0.18	0.54	1.03	1.76	0.18	0.54	1.23	2.10
0.045	0.2	0.045	0.24	0.05	0.14	0.27	0.46	0.05	0.14	0.32	0.55

Table 4　Identifications of cavitation modes by Yoshida et al. (2001) (f_n : Shaft rotational speed)

Cavitation Mode	Mode Frequency (Hz)	
	Inducer (A): Z=2	Inducer (B): Z=4
Equal Length Cavitation	$2.0f_n$	$4.0f_n$
Alternate Blade Cavitation	$1.0f_n$	$20f_n$
Rotating Cavitation	1.1–1.5f_n	
Cavitation Surge	5–10 Hz	

each tested case for both impellers are summarized in Table 3.

4. Event Detection Technique

The cavitation modes of fluctuating pressures at inlet locations are analyzed by using a cross-spectral density. The mode frequency is determined by the blade passage frequency (BPF) and the phase angle (δ) at a specified Strouhal number.

$$f_m = \frac{\delta \times St \times BPF}{360} \qquad (5)$$

The number of cavity (m) is computed by the phase angle (δ) and the separation angle ($\Delta\theta$) between two sensors at inlet locations (Crane et al., 1995):

$$m = \frac{\delta}{\Delta\theta} \qquad (6)$$

Yoshida et al. (2001) classified the cavitation mode frequencies of inducer as a function of shaft rotational frequency (f_n) as shown in Table 4. They estimated the cavity length dependent upon cavitation number and incidence angle in each region.

The conditional sampling techniques have been used to examine the large-amplitude pressure events at wall in a time domain. Short-Time Fourier Transform (STFT), Continuous Wavelet Transform (CWT), and Wigner-Ville distribution have been used as the time-frequency localization procedures. The STFT method uses a constant time-frequency resolution for both high and low frequencies. The CWT method improves the low-frequency characteristics and time resolution to analyze the specified signals such as energy flows and sound signals, but still encounters difficulties when analyzing the fine signals. The Wigner-Ville distribution method resolves the window-size constraints and applies the Kernel function to eliminate the counterfeit signals.

To analyze the local time-frequency characteristics at outlet location for each cavitation number, Choi-Williams (C-W) distribution was employed in this research, as suggested by Lee and White (1998). The general form of a bilinear transformation used in the time-frequency analysis is given as follows:

$$S(t, f) = \int_{-\infty}^{\infty}\int_{-\infty}^{\infty} \Phi(u-t, \tau)$$
$$x\left(u+\frac{\tau}{2}\right)x^*\left(u-\frac{\tau}{2}\right)e^{-j2\pi ft}dud\tau \qquad (7)$$

where $\Phi(t, \tau)$ is a smoothing kernel function. The Choi-Williams distribution is defined, using the exponential kernel, as follows:

$$W(t, f) = \int_\tau e^{-j2\pi ft} \int_u \frac{1}{2\tau} \sqrt{\frac{\sigma}{\pi}} e^{-j2\pi(ft+\sigma(u-t)^2/4\tau^4)}$$
$$x\left(u+\frac{\tau}{2}\right)x^*\left(u-\frac{\tau}{2}\right)e^{-j2\pi ft} du d\tau \quad (8)$$

where $\sigma(>0)$ is used as a scaling parameter and a kernel shape coefficient.

To correlate the time-frequency pattern at each station, time signals were high-pass filtered, bilinear-transformed using the C-W kernel function, and ensemble-averaged. The time-frequency characteristics of wall pressures at outlet location are analyzed in terms of the event frequencies, duration times, and the number of events by using the C-W distribution in this paper.

5. Cavitation Mode Analysis of Inducers and B

5.1 Inducer A

The cross-spectral density functions and Wigner-Ville distributions are analyzed for the cases of $\Phi=0.30$ (Figs. 6, 7, and 8) and $\Phi=0.35$ (Figs. 9, 10, and 11) by controlling the cavitation number (σ) at the inlet of inducer A, as given in Table 3.

At the flow coefficient of 0.30, the incidence angle is computed as $6.8°$. At a cavitation number of 0.3, the cavitation seems to be the equal length cavitation with a frequency of $2.1f_n$, as shown in
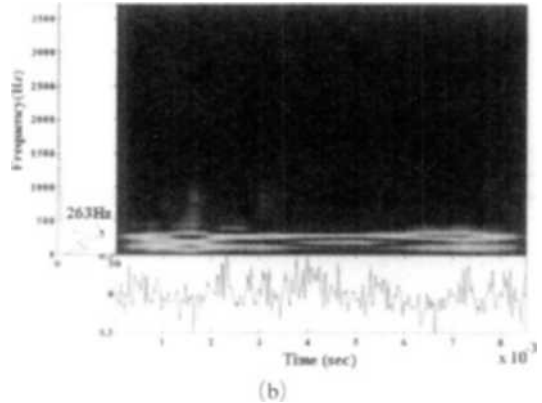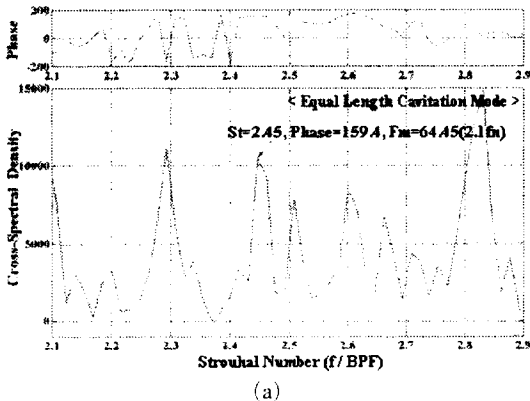

Fig. 6 Cavitation event characteristics at $NPSH_a=7.72$ m and $\Phi=0.30$ for inducer A : (a) cross-spectral density function at inlet ; (b) Choi-Williams distribution at outlet.
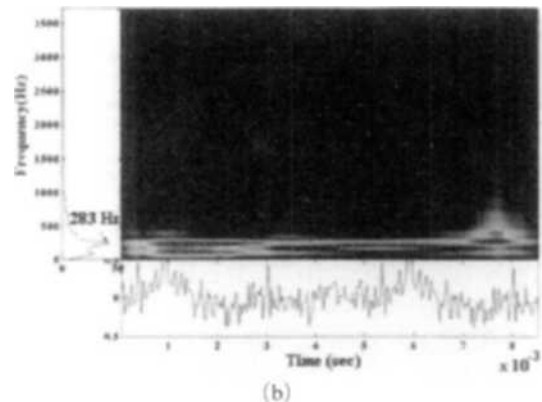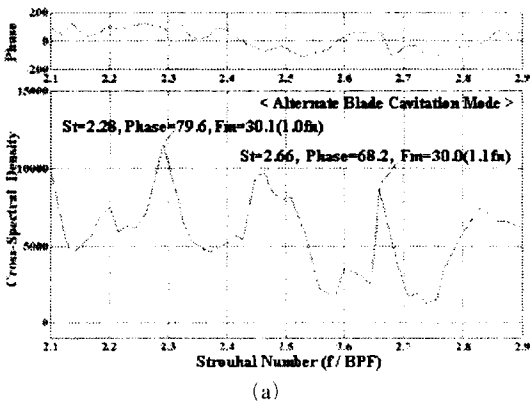

Fig. 7 Cavitation event characteristics at $NPSH_a=6.35$ m and $\Phi=0.30$ for inducer A : (a) cross-spectral density function at inlet ; (b) Choi-Williams distribution at outlet
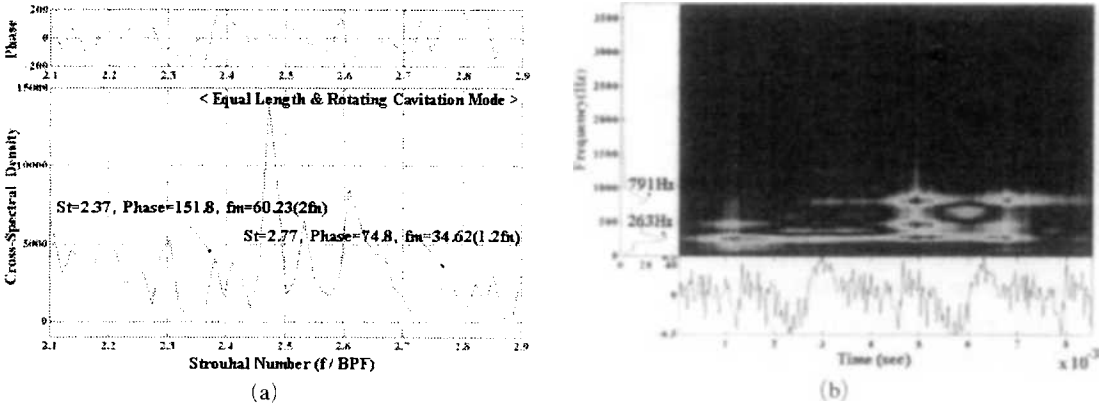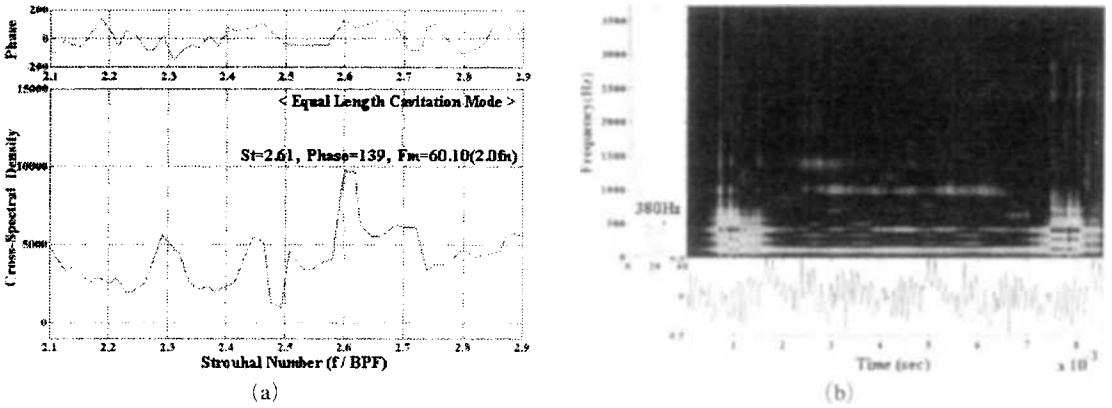
Fig. 8 Cavitation event characteristics at NPSH$_a$=5.0 m and Φ=0.30 for inducer A : (a) cross-spectral density function at inlet ; (b) Choi-Williams distribution at outlet.

Fig. 9 Cavitation event characteristics at NPSH$_a$=7.79 m and Φ=0.35 for inducer A : (a) cross-spectral density function at inlet ; (b) Choi-Williams distribution at outlet.
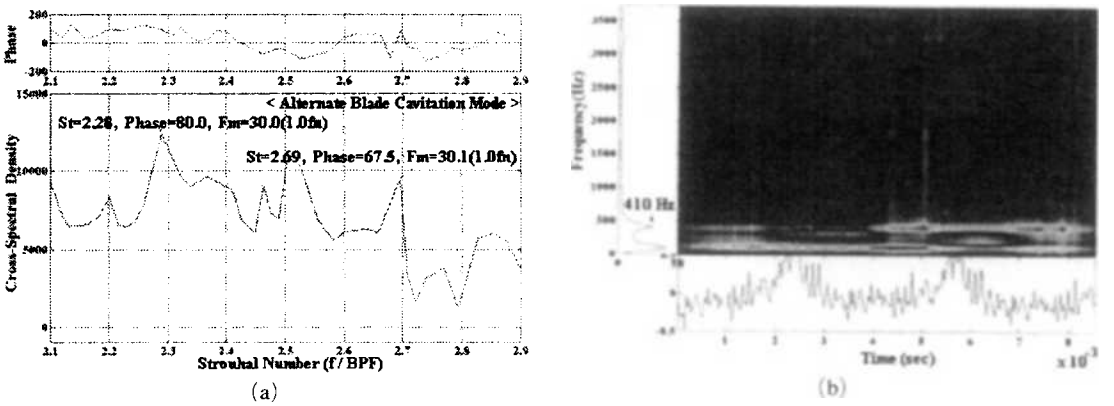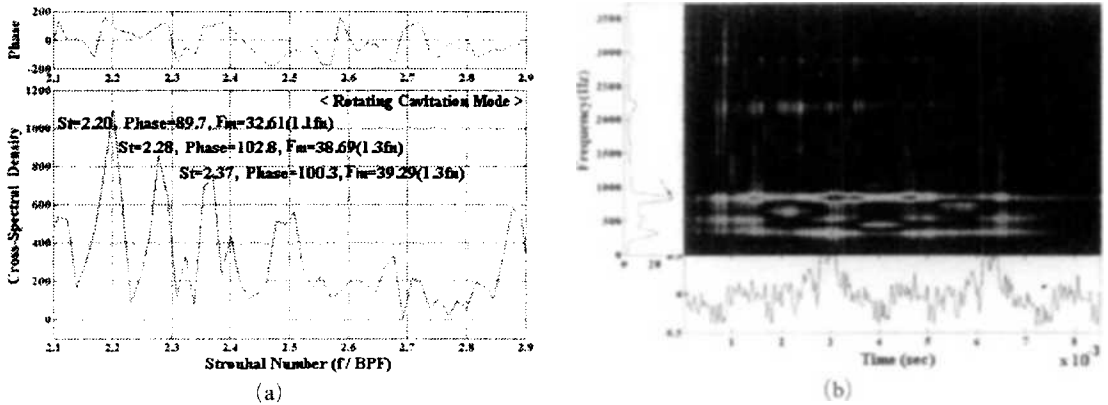

Fig. 10 Cavitation event characteristics at NPSH$_a$=6.43 m and Φ=0.35 for inducer A : (a) cross-spectral density function at inlet ; (b) Choi-Williams distribution at outlet.

Fig. 11 Cavitation event characteristics at NPSH$_a$=5.07 m and Φ=0.35 for inducer A : (a) cross-spectral density function at inlet ; (b) Choi-Williams distribution at outlet.

Fig. 6(a). In this case the cavitation length was estimated to be 0.42 S at the tip of the inducer. Two cavitation events of 263 Hz were detected at the exit of inducer with approximately equal duration of 3.5 ms as shown in Fig. 6(b).

The alternate cavitation mode, with cavity lengths of 0.4 S and 0.17 S at the tip, was observed at the cavitation number of 0.17 as shown in Fig. 7(a). Two events having the duration lengths of 3.0 ms and 1.0 ms were detected at a frequency of 283 Hz as shown in Fig. 7(b). At a reduced inlet pressure of σ equal to 0.045, the mixed mode of equal length and rotating cavitations occurred. The event of 2 ms duration at 263 Hz and the rotating event at 791 Hz can be identified in Fig. 8(b).

At a flow coefficient of 0.35, the incidence angle was computed as 5.4°. At a cavitation number 0.3, the cavitation appears to be equal length mode with a frequency of 2.0f$_n$ as shown in Fig. 9(a). For this case, the steady cavitation length was estimated as 0.35 S at the tip of the inducer. Two cavitation events of 380 Hz were detected at the exit of inducer with approximately equal duration length of 1.0 ms as shown in Fig. 9(b).

Figure 10(a) revealed the alternate cavitation mode having the cavity lengths at the tip as 0.58 S and 0.50 S at σ=0.17 and $\sigma/2\alpha$=0.9. Two events having the duration lengths of 1.0 ms and 1.5 ms were detected at the frequency of 410Hz as shown in Fig. 10(b). At a reduced inlet pressure of σ equal to 0.045, the rotating cavitation oc-

curred. The unsteady rotating events at 849 Hz can be noticed in Fig. 11(b). The event frequency, its duration length, and number of events detected at the outlet of inducer A by Choi-Williams distribution are summarized in Table 6.

5.2 Inducer B

The cross-spectral density functions and Wigner-Ville distributions were also analyzed for the cases of Φ=0.10 (Figs. 12, 13, and 14) and Φ=0.13 (Figs. 15, 16, and 17) by controlling the cavitation number (σ) at the inlet of inducer B as given in Table 3. By considering the cross-flow effect in a swept inducer (Acosta et al., 2000), the alternate blade cavitation was reported to occur at $\sigma_c/(2\alpha_c) \approx 0.9$ and to shift to unsteady cavitation at $\sigma_c/(2\alpha_c) \approx 0.4$.

At a flow coefficient of Φ=0.10, the incidence angle was computed as 5.1°. Figure 12(a) showed the cavitation mode of 4.0f$_n$, close to the equal length cavitation of four-bladed inducer, having steady cavity length at the tip as 0.20 S at the cavitation number of 0.32. Two cavitation events of 263 Hz were shown in Fig. 12(b) at the exit of inducer with approximately equal duration of 2.3 ms.

Figure 13(a) revealed same cavitation mode as the case of cavitation number of 0.32 except having cavity length at the tip as 0.40 S at the cavitation number of 0.18, where the correlation value of $\sigma_c/(2\alpha_c)$ suggested that alternate cavitation occurred. Two events of approximately
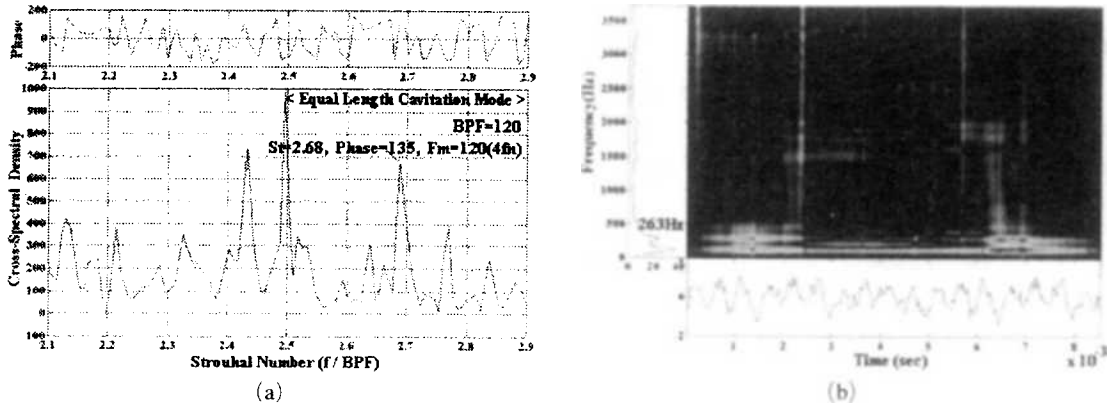
Fig. 12 Cavitation event characteristics at $NPSH_a = 3.23$ m and $\Phi = 0.10$ for inducer B : (a) cross-spectral density function at inlet ; (b) Choi-Williams distribution at outlet.
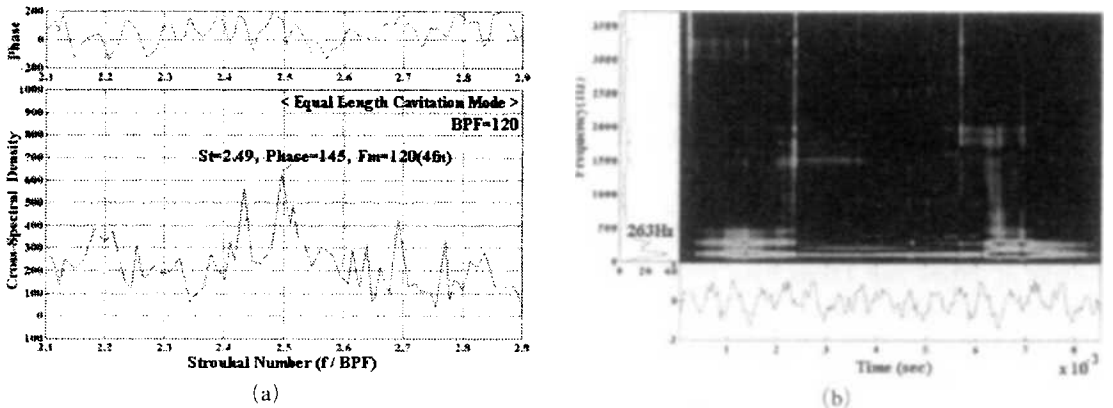

Fig. 13 Cavitation event characteristics at $NPSH_a = 1.87$ m and $\Phi = 0.10$ for inducer B : (a) cross-spectral density function at inlet ; (b) Choi-Williams distribution at outlet.
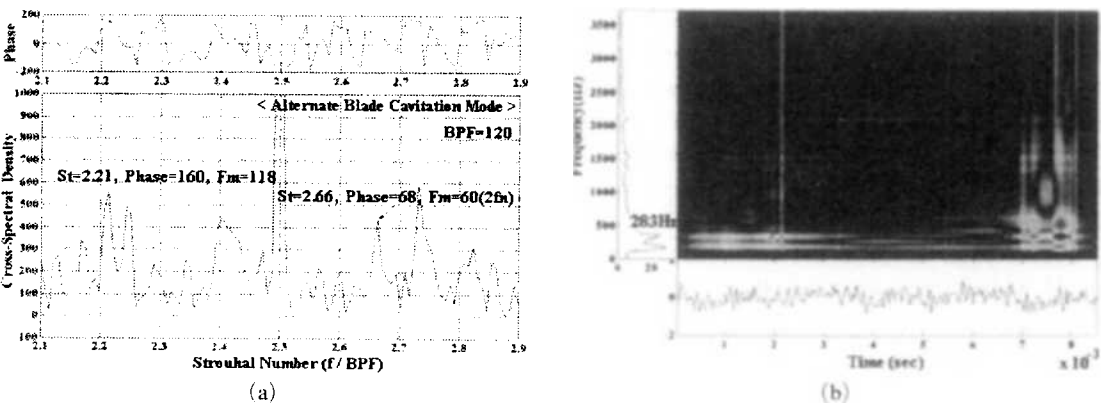

Fig. 14 Cavitation event characteristics at $NPSH_a = 0.51$ m and $\Phi = 0.10$ for inducer B : (a) cross-spectral density function at inlet ; (b) Choi-Williams distribution at outlet.
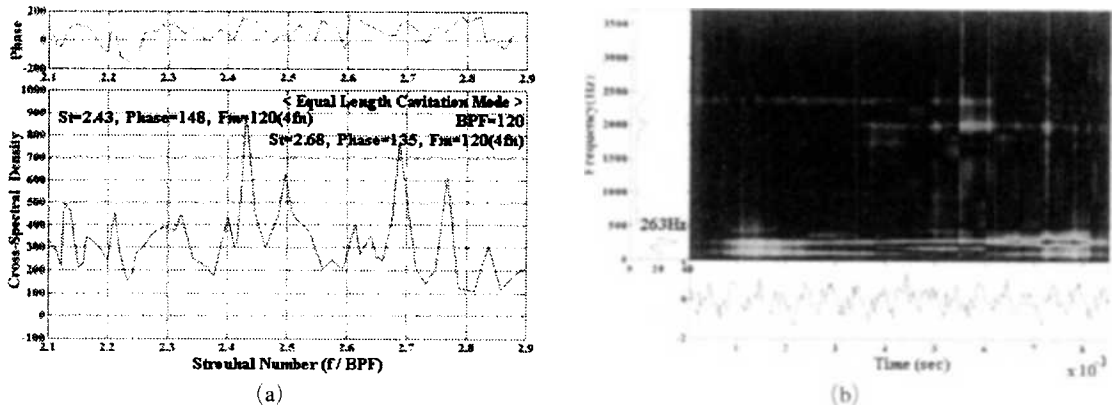
Fig. 15 Cavitation event characteristics at NPSH$_a$=3.25 m and Φ=0.13 for inducer B : (a) cross-spectral density function at inlet ; (b) Choi-Williams distribution at outlet.
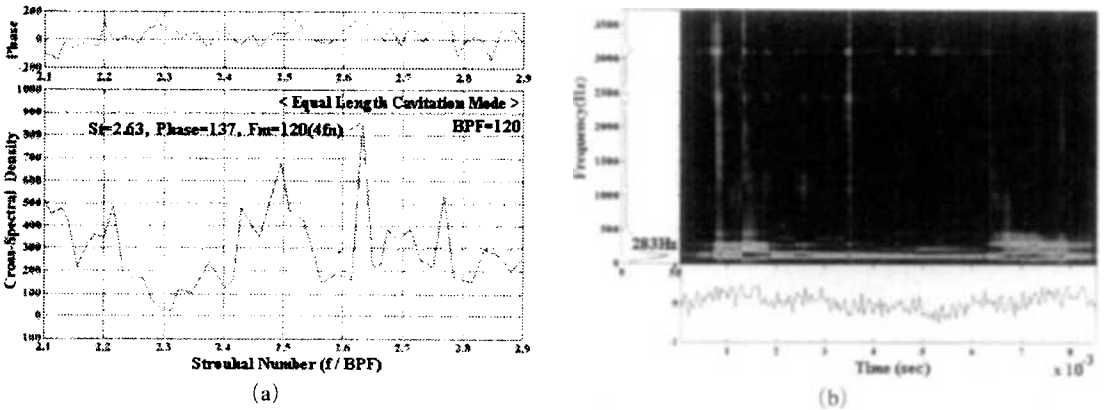

Fig. 16 Cavitation event characteristics at NPSH$_a$=1.89 m and Φ=0.13 for inducer B : (a) cross-spectral density function at inlet ; (b) Choi-Williams distribution at outlet.
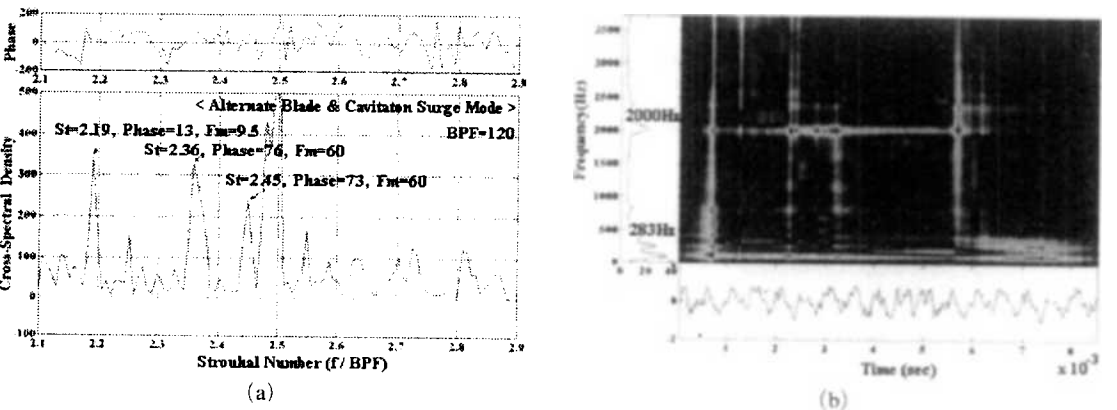

Fig. 17 Cavitation event characteristics at NPSH$_a$=0.53 m and Φ=0.13 for inducer B : (a) cross-spectral density function at inlet ; (b) Choi-Williams distribution at outlet.

equal duration of 2.5 ms were detected at the frequency of 263 Hz as shown in Fig. 13(b). The alternating cavitation mode having cavity lengths at the tip as 0.65 S and 0.12 S were observed at a reduced inlet pressure of σ equal to 0.05. Two events having duration of 1.6 ms and 3.0 ms occurred at a frequency of 283 Hz as shown in Fig. 14(b).

The incidence angle, α, was computed as 4.3° at a flow coefficient of $\Phi=0.13$ for inducer B. Figure 15(a) showed the cavitation mode frequency, $4.0f_n$, of equal length cavitation having steady cavity length at the tip as 0.1 S at the cavitation number of 0.32. Two cavitation events of 263 Hz were detected at the exit of inducer with approximately equal duration of 3.2 ms as shown in Fig. 15(b).

Figure 16(a) revealed the equal-length cavitation mode having cavity length at the tip as 0.35 S at $\sigma=0.18$ and $\sigma_c/(2\alpha_c)=2.10$. Two events

of approximately equal duration of 2.1 ms were detected at a frequency of 283 Hz as shown in Fig. 16(b). At a reduced inlet pressure of σ equal to 0.05, the mixed mode of alternate blade cavitation and cavitation surge occurred. The alternating cavitation mode was observed to have cavity lengths at the tip as 0.40 S and 1.25 S. Two events of duration of 1.0 ms and 2.8 ms, and cavitation surge event were detected at frequencies of 283 Hz and 2000 Hz, respectively, as shown in Fig. 17(b). The event frequency, its duration, and number of events detected at the outlet of inducer B by Choi-Williams distribution were summarized in Table 8.

As the cavitation number decreased, the equal-length cavitation, alternate-blade cavitation, rotating cavitation, and/or cavitation surge were orderly observed, depending on the flow coefficients, as shown in Tables 5 and 7 for the test inducers A and B, respectively. The cavitation

Table 5   Summary of inlet modes of inducer (A) at $\Phi=0.30$, 0.35 (E : Equal length, A : Alternate blade, R : Rotating, S : Surge)

	$\Phi=0.3$			$\Phi=0.35$		
	Modes	Cell No.	Cavity Length	Modes	Cell No.	Cavity Length
$\sigma=0.300$	E	1.8	0.42 S	E	1.5	0.35 S
$\sigma=0.170$	A	0.8	0.40 S/0.17 S	A	0.9/0.8	0.58 S/0.50 S
$\sigma=0.045$	E+R	1.7, 0.8	Unsteady	R	1.0/1.1	Unsteady

Table 6   Summary of events at outlet of inducer (A) by Choi-Williams distribution for one quarter of period

	$\Phi=0.3$			$\Phi=0.35$		
	Frequency (Hz)	Duration (msec)	No. of event	Frequency (Hz)	Duration (msec)	No. of event
$\sigma=0.300$	263	3.5	2	380	1.0	2
$\sigma=0.170$	283	3.0/1.0	2	410	1.0/1.5	2
$\sigma=0.045$	263, 791	2.0/0.5	2, 2	849	5.0	4

Table 7   Summary of inlet modes of inducer (B) at $\Phi=0.10$, 0.13 (E : Equal length A : Alternate blade R : Rotating S : Surge)

	$\Phi=0.1$			$\Phi=0.13$		
	Modes	Cell No.	Cavity Length	Modes	Cell No.	Cavity Length
$\sigma=0.320$	E	1.5	0.2 S	E	1.5/1.6	0.1 S
$\sigma=0.180$	E	1.6	0.4 S	E	1.5	0.35 S
$\sigma=0.050$	A	0.8	0.65 S/1.12 S	A+S	50.8, All	0.40 S/1.25 S

Table 8 Summary of events at outlet of inducer (B) by Choi-Williams distribution for one quarter of period

	$\Phi=0.1$			$\Phi=0.13$		
	Frequency (Hz)	Duration (msec)	No. of event	Frequency (Hz)	Duration (msec)	No. of event
$\sigma=0.320$	263	2.3	2	263	3.2	2
$\sigma=0.180$	263	2.5	2	283	2.1	2
$\sigma=0.050$	283	1.6/3.0	2	283, 2000	1.0/2.8	2, 3

events were observed to move to higher frequencies at the exit of inducer when the operating flow coefficient was increased. Furthermore, the equal-length cavity lengths got shorter and the event duration at exit became shorter with events occurring at higher frequencies for the higher flow coefficient. At the same flow coefficient, the equal length cavitation showed the general trend of the longer cavity length and event duration time at the exit at a smaller cavitation number.

6. Conclusion

Exposing on cavitation for quite a period of time makes pump impellers and casing permanently damaged. Most of the inducer is designed at a maximum efficiency point of the pump, therefore the decrease of suction performance, due to the effects of flow separation, and inlet inverse flow at off-design points is often observed. The time-frequency characteristics of wall pressures at off-design points for an industrial inducer and the inducer used in LE-7 engine of H-2 rocket were analyzed by using Choi-Williams distribution in an effort to detect the onset of cavitation and identify cavitation mode.

The cavitation events were found to move to higher frequencies at the exit of inducer when the flow coefficient was increased. It was observed that the cavity length of surface cavitation at various conditions were closely correlated with the modified cavitation number $(\sigma_c/2\alpha_c)$ and event duration both for inducer A (without sweep) and inducer B (with backward sweep), but the observed modes were inconsistent with the mode predicted by linear cascade analysis in the cross-flow plane at far off-design points. It can be addressed that this event detection technique

downstream of the pump impeller may serve as a condition-monitoring algorithm integrated with a knowledge-based system to detect the cavitaion mode in the pump system.

Acknowledgment

References

Acosta, A. J., 1955, *A Note on Partial Cavitation of Flat Plate Hydrofoils*, Caltech Hydro Lab. Report No. E-19.9.

Acosta, A. J., Tsujimoto, Y., Yoshida, Y., Azuma, S. and Cooper, P., 2000, "Effects of Leading Edge Sweep of the Cavitating Characteristics of Inducer Pumps," *ISROMAC-8*.

Crane, M. H., Bent, P. H. and Quinlan, D. A., 1995, "Rotating Instability Waves as a Noise Source in a Ducted Axial Fan," *Proceedings of the ASME Noise Control and Acoustics Division*, pp. 25~26.

Horiguchi, H., Watanabe, S., Tsujimoto, Y. and Aoki, M., 2000, "A Theoretical Analysis of Alternate Blade Cavitation in Inducers," *ASME J. Fluids Eng.*, Vol. 122, No. 1, pp. 156~163.

Kubota, A., Kato, H., Yamaguchi, H. and Maeda, M., 1989, "Unsteady Structure Measurement of Cloud Cavitation on a Foil Section Using Conditional Sampling Technique," *Trans. ASME I : J. of Fluid Eng.*, Vol. 111, pp. 204~210.

Lee, S. K. and White, P. R, 1998, "The Enhanced of Impulsive Noise and Vibration Signals for Fault Detection in Rotating and

Reciprocating Machinery," *J. of Sound and Vib.*, Vol. 217(3), pp. 485~505.

Yoshida, Y., Tsujimoto, Y., Kataoka, D., Horiguchi, H. and Wahl, F., 2001, "Effects of Alternate Leading Edge Cutback on Unsteady Cavitation in 4-bladed Inducers," *ASME J. Fluids Eng.*, Vol. 123, No. 4, pp. 762~770.